

Measurement of the radon concentration in purified water in the Super-Kamiokande IV detector

Y. Nakano^{a,*}, T. Hokama^b, M. Matsubara^c, M. Miwa^d, M. Nakahata^{e,f}, T. Nakamura^g,
H. Sekiya^{e,f}, Y. Takeuchi^{a,f}, S. Tasaka^e, R.A. Wendell^{h,f}

^aDepartment of Physics, Graduate School of Science, Kobe University, Kobe, Hyogo 657-8501, Japan

^bNuclear Emergency Assistance and Training Center, Japan Atomic Energy Agency, Ibaraki 311-1206, Japan

^cHead Office for Information and Management, Gifu University, Gifu 501-1193, Japan

^dDivision of Radioisotope Experiment, Life Science Research Center, Gifu University, Gifu 501-1193, Japan

^eKamioka Observatory, Institute for Cosmic Ray Research, The University of Tokyo, Gifu 506-1205, Japan

^fKavli Institute for the Physics and Mathematics of the Universe (WPI),

The University of Tokyo Institutes for Advanced Study, The University of Tokyo, Kashiwa, Chiba 277-8583, Japan

^gDepartment of Physics, Faculty of Education, Gifu University, Gifu 501-1193, Japan

^hDepartment of Physics, Kyoto University, Kyoto, Kyoto 606-8502, Japan

Abstract

The radioactive noble gas radon can be a serious background source in the underground particle physics experiments studying processes that deposit energy comparable to its decay products. Low energy solar neutrino measurements at Super-Kamiokande suffer from these backgrounds and therefore require precise characterization of the radon concentration in the detector's ultra-pure water. For this purpose, we have developed a measurement system consisting of a radon extraction column, a charcoal trap, and a radon detector. In this article we discuss the design, calibration, and performance of the radon extraction column. We also describe the design of the measurement system and evaluate its performance, including its background. Using this system we measured the radon concentration in Super-Kamiokande's water between May 2014 and October 2015. The measured radon concentration in the supply lines of the water circulation system was 1.74 ± 0.14 mBq/m³ and in the return line was 9.06 ± 0.58 mBq/m³. Water sampled from the center region of the detector itself had a concentration of < 0.23 mBq/m³ (95% C.L.) and water sampled from the bottom region of the detector had a concentration of 2.63 ± 0.22 mBq/m³.

Keywords: Super-Kamiokande, Radon, Solar neutrino, Charcoal, Radon extraction column

1. Introduction

The framework of three-flavor neutrino oscillations [1, 2] is increasingly well understood. However, there remain unknown quantities, including the absolute scale of the neutrino mass states and whether CP symmetry is violated in neutrino mixing. Hints of oscillations among solar neutrinos were first obtained from the difference between the solar-neutrino fluxes measured with the elastic-scattering channel at Super-Kamiokande (Super-K) and the charged-current channel at

*Corresponding author. Tel: +81 78 803 5640; Fax: +81 78 803 5662.

Email address: ynakano@phys.sci.kobe-u.ac.jp (Y. Nakano)

the Sudbury Neutrino Observatory (SNO) in 2001 [3, 4]. Though only electron neutrinos are produced in the core of the Sun, this result demonstrated the existence of other neutrino components in the solar neutrino flux. Solar neutrino oscillations were subsequently confirmed by including neutral-current measurements from SNO [5]. Precise solar neutrino oscillation measurements require large statistics and Super-K provided such measurements with its large detector volume [6–9]. Its large size further benefits Super-K’s efforts to test for the presence of solar and terrestrial matter effects in the solar neutrino oscillations as predicted by Mikheyev, Smirnov and Wolfenstein [10, 11], the so-called MSW effect. Although the MSW effect is enough to explain the current solar neutrino data, direct evidence for it has not yet been obtained. At Super-K, it manifests as a distortion in the energy spectrum of recoiling electrons produced by solar neutrino interactions in water. Measurements of the electron recoil energy spectrum and the asymmetry of the solar neutrino interaction rate during the day and during the night [12] allow Super-K to directly probe the matter effects in the Sun and Earth, respectively.

Moreover, this distortion is expected to increase at lower energies (the so-called “upturn”) and therefore requires an energy threshold that is as low as possible. At Super-K, the energy threshold is limited by radioactive backgrounds, most of which arise from radon (Rn) contamination in the detector water [13]. In order to achieve a suitably low background for solar neutrino analysis at the lowest energies, the Rn emanation from all components of the Super-K detector must be reduced. For this purpose, we have developed a new measurement system to monitor the Rn concentration in purified water. Herein we present details of the system as well as results of in-situ measurements at Super-K.

This paper is organized as follows. In Section 2 we describe the Super-K detector and its water system as well as summarize the history of Rn studies at Super-K. Section 3 presents a new method of extracting Rn from water and subsequently describes the design and data analysis of a system to measure the extracted Rn. We discuss background levels and systematic uncertainties accompanying this measurement in Section 4 before presenting measurement results in Section 5. In Section 6, we discuss several possible Rn sources in the Super-K tank. Finally in Section 7, we conclude this study and outline prospects for the future. Note that we use the term Rn to refer specifically to ^{222}Rn in this paper, unless otherwise stated.

2. The Super-Kamiokande detector

Super-K is a water Cherenkov detector containing 50000 tonnes of highly purified water that is viewed by 11129 20-inch photomultiplier tubes (PMTs) [14]. It is located roughly 1000 m underground (2700 m water equivalent) inside the Ikenoyama mountain in Gifu prefecture, Japan. We define the local coordinate system of the detector as (x, y, z) , where (x, y) represents the plane of the cylinder as viewed from above and z represents the height within the detector tank [14]. The origin is placed at the center of the tank.

After the installation of new front end electronics in 2008 [15], the fourth phase of Super-K (SK-IV) started and was concluded 10 years later in May 2018. With improvements in the water circulation system, calibration methods [16], and event selection, the detector’s energy threshold was lowered to 3.5 MeV in terms of electron recoil kinetic energy [9]. These upgrades have also allowed for precision measurements of the electron recoil energy spectrum and the Super-K data together with data from SNO provide the strongest constraint on the solar electron neutrino survival probability [9, 17]. However, experimental data from other solar neutrino experiments, including radiochemical experiments [18–20], water Cherenkov experiments [21–24], and liquid scintillator experiments [25–31] have not yet demonstrated the upturn of the

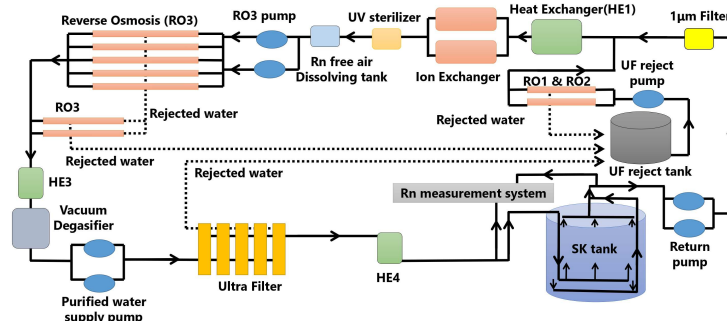


Figure 1: Schematic diagram of the SK-IV water system. Purified water is supplied through inlets at the bottom and drained from outlets in both the bottom and top regions as shown in details in Fig. 2.

recoil energy spectrum expected from the MSW effect. This null observation has motivated several theoretical explanations including models with sterile neutrinos [32–34], mass-varying neutrinos [35], and non-standard interactions [36, 37].

At energies below 5 MeV Super-K has observed an excess of events close to the detector structure near the bottom and barrel regions of the detector [9]. However, due to the limited energy resolution of the detector [13], this energy region overlaps with that of the primary background due to electrons from the β decay of ^{214}Bi (Rn daughter). The Q -value of this decay is $E_{\beta}^{\text{max}} = 3.27$ MeV. In order to understand this background and its contribution to the analysis of solar neutrinos, precise measurements of the Rn concentrations in the water of SK-IV detector and in the outputs of the system are necessary.

2.1. Water purification system

The original water purification system for Super-K has been described in Ref. [38]. During the first phase of Super-K (SK-I), it consisted of mechanical $1\ \mu\text{m}$ filters, a heat exchanger (HE1), mixed-bed de-ionization resins (Ion Exchanger, IE), ultraviolet (UV) sterilizers, a vacuum degasifier (VD), a high-quality IE (Cartridge Polisher, CP), and ultrafilters (UF). Their ordering here is the same as that of their appearance in the recirculation process. Over the intervening 20 years, the system has been continuously upgraded to reduce impurities and improve control over the detector environment. For example, a reverse-osmosis membrane (RO) was added to the recirculation line during the second phase of operations (SK-II), and an additional heat exchanger (HE3) was installed during the third phase (SK-III). Furthermore, at the beginning of SK-IV an upgraded heat exchanger (HE4) was added to system in order to further control the input water temperature and thereby suppress convection in the tank water, which causes Rn and other impurities to mix into the fiducial region of the detector (details below). Afterwards the water temperature is controlled at 13.06°C with an accuracy of 0.01°C [16, 39]. The total circulation rate during SK-IV was 60 ton/h, which doubles that of SK-III. Fig. 1 shows the configuration of the system at the end of SK-IV.

Water is supplied to Super-K through inlets at the bottom region of the inner detector (ID), which is shown in Fig. 2. The inlets extend up to $z = -16.5$ m in the tank, which is 40 cm below the bottom edge of the fiducial volume used for analysis [9]. The ID is separated optically from the outer detector (OD) by a Tyvek sheet [16], but the water in the tank still flows from ID to OD. As shown in Fig. 2, water is drained through outlets placed at the top region of the tank and

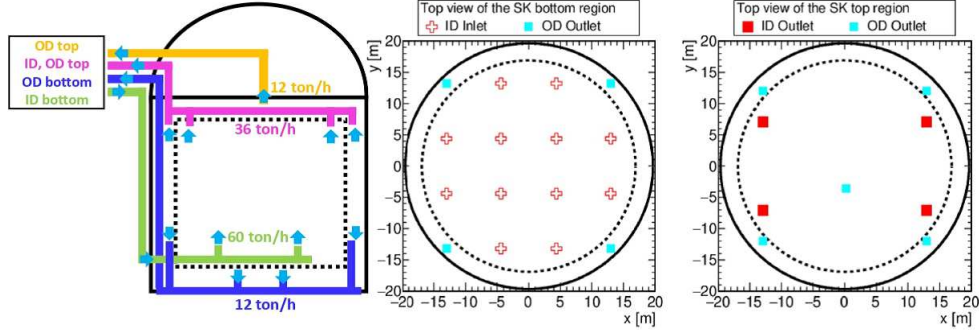


Figure 2: Left: Schematic view of the water circulation paths in the Super-K tank. The solid line shows the Super-K water tank, and the dashed line shows the inner detector. The arrows show the direction of water flows. Middle and Right: The locations of the water inlets and outlets at the bottom (top) of the Super-K tank. The x and y coordinate axes are drawn as defined in Ref. [14]. The middle figure illustrates their locations in the bottom region, and the right figure illustrates their locations in the top region. The solid circles describe the Super-K water tank, while the dashed circles outline the inner detector in the tank. The outlets placed in the OD region drain the water from the “OD barrel” region.

at the bottom region of the OD for recirculation and purification. The outlets placed in the OD drain water from its barrel region (“OD barrel”).

There are twelve inlets placed at the bottom of ID and four outlets placed in OD. As a result of this configuration and the precise temperature control enabled by HE4, the water tank above $z = -11$ m experiences laminar flow, and therefore lower Rn backgrounds, while that below this level undergoes convection [16].

2.2. History of Rn studies at Super-K

Several techniques for evaluating the Rn and radium (^{226}Ra) concentrations in water have been developed for underground experiments [40–47]. In particular, a Rn assay system for the Super-K water was developed during SK-I [48]. The sensitivity of that detector is 0.7 mBq/m^3 for a single-day measurement and is limited by statistical fluctuations in the background count rate. Using that system, the Rn concentration in the supply water was measured to be $0.4 \pm 0.2 \text{ mBq/m}^3$ in 2001, while that in the tank water itself was $< 2.0 \text{ mBq/m}^3$ [14]. This was the last of such measurements prior to the results discussed below. In order to understand the Rn concentration sufficiently, we require sensitivity to the Rn concentration in purified water at the 0.1 mBq/m^3 level.

3. Experimental setup

In order to measure ultra-low levels of Rn in water, Rn must first be extracted into air so that daughters of Rn (especially, ^{218}Po and ^{214}Po) can be electrostatically collected in air because they tend to have a positive charge [49]. This technique requires efficient Rn extraction as well as trapping to allow enough atoms to be collected during a measurement. To accomplish this we have developed a new water-air extraction column and have expanded on the 80 L electrostatic detection system detailed in [50, 51] by introducing a chilled charcoal trap to enhance the Rn collection. The accumulated Rn is released and transferred to a detector, whose sensitivity is typically 0.5 mBq/m^3 in air for a single-day measurement [50]. Finally, an overall sensitivity

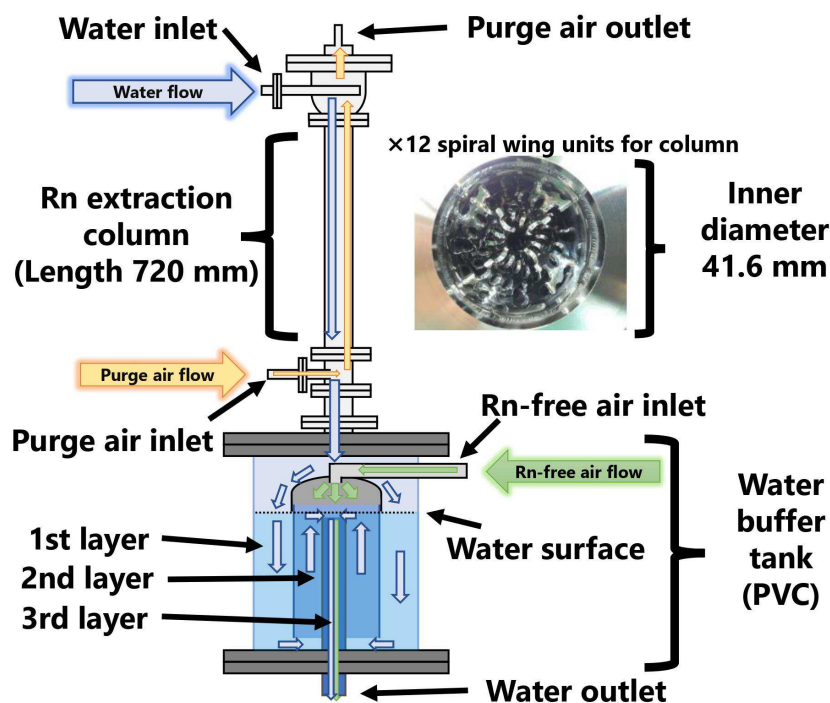


Figure 3: Schematic diagram of the Rn extraction system. The top (bottom) part of the system is the extraction column (water buffer tank). Numerical values give lengths in millimeters (mm), while solid (open) arrows show the flow of sampled water (purge air).

of $\sim 0.1 \text{ mBq/m}^3$ in water has been achieved as determined by fits to the shape of the Rn decay curve. This represents an order of magnitude improvement over the previous systems [38, 48].

3.1. Column for radon extraction

Fig. 3 shows a schematic diagram of the extraction column, which mixes flowing water with purge gas (air) to extract Rn. The extraction column consists of 12 spiral wing units and is equipped with inlets for both the purge air and the sampled water as well as outlets for Rn-degassed water and purge air. A buffer tank is located below the column to store Rn-degassed water.

The spiral wing unit¹ is a combination of six right-turn units and six left-turn units, which are welded to each other alternately. The inside of a wing unit has four welded wings that are directed downward with a height, inner diameter, and outer diameter of 60.0 mm, 41.6 mm and 48.6 mm, respectively. Each wing contains several holes to improve its Rn extraction efficiency. The surfaces of the wings and holes have been electro-polished in order to reduce emanation of Rn from their surfaces.

Degassed water passing through the extraction column is collected in the buffer tank. The tank is made of transparent polyvinyl chloride (PVC), so the water level can be monitored. In

¹The unit itself is constructed with a MU-reactorTH, a product of the MU Co., Ltd. http://www.mu-company.com/en_index.html

order to prevent gasses from the external environment from entering into the extraction column, the tank is divided into three layers (1st, 2nd and 3rd layers shown in Fig. 3) and Rn-free air is supplied to the innermost 3rd layer during operations. The degassed water is finally drained from the pipe of water outlet (the 3rd layer in Fig. 3). This design allows the extraction column to maintain both the water level and the inner pressure at the 1st layer.

Urethane gaskets have been used between the extraction column and water tank here since this material was found to emanate less Rn [39, 44] though EPDM (ethylene propylene diene monomer) or butyl gaskets are commonly used to connect pipes in such systems.

Sampled water enters through the water inlet at the top and at the same time purge air enters the extraction column through the purge air inlet. When the sampled water falls down through the extraction column and strikes its wings, the water is turned into mist allowing the dissolved Rn to escape into the air and be transported out of the system via the upper air outlet.

The total amount of Rn in the water and in the air during this process is conserved before and after the extraction, as expressed by the following equation:

$$C_{w,0}F_w + C_{a,0}F_a = C_wF_w + C_aF_a. \quad (1)$$

Here $C_{w,0}$ ($C_{a,0}$) is the Rn concentration of the sampled water (purge air) before extracting in units of Bq/L, C_w (C_a) is that of degassed water (purge air) after extracting, and F_w (F_a) is the flow rate of the water (air) through the system in units of L/min.

In order to evaluate the Rn extraction efficiency, we rewrite Eq. (1) as follows:

$$\begin{aligned} C_{w,0}F_w &= C_wF_w + (C_a - C_{a,0})F_a, \\ 1 &= \frac{C_w}{C_{w,0}} + \frac{C_a - C_{a,0}}{C_{w,0}} \times \frac{F_a}{F_w}. \end{aligned} \quad (2)$$

The second term on the right side in Eq. (2) can be regarded as the Rn extraction efficiency of the system. Note that the total amount of extracted Rn depends on the flow rates of the sampled water and the purge air. Accordingly, the factor (F_a/F_w) in the second term is required to normalize the extraction efficiency by taking into account the total volume of water and air used in the Rn extraction (mixing) process. It can be determined by measuring the Rn concentrations in both the sampled water and the purge air before and after the extraction process.

To determine the Rn extraction efficiency, we built a calibration system at Gifu University as shown in Fig. 4. The system consists of a 70 L Rn detector [38], an air mass-flow controller (HORIBA STEC Z512), two pressure gauges (Naganokeiki Co. Ltd. ZT67), a water mass-flow controller (TOFCO Corp. FLC620), an electrical dehumidifier (KELK DH-209C), an air pump, and an ionization chamber (OHKURA ELECTRIC Co. Ltd. RD1210B).

Purge air for the calibration was taken from environment air at Gifu University and had a typical Rn concentration of ~ 0.01 Bq/L as measured by the 70 L Rn detector. After the extraction, the concentration in the outflow air was measured with the ionization chamber. Tap water from the university was used as the Rn source. Its Rn content was measured with a liquid scintillator counter (LSC) system (Tri-Crab 2900TR produced by PerkinElmer Inc.), as is standard for evaluation of hot spring water [52–54], and was found to be 5–7 Bq/L. The pressure inside the extraction column was monitored by two pressure gauges, located at the inlet and the outlet of the extraction column, because the Rn extraction efficiency may depend on this quantity. The electric dehumidifier was installed just after the extraction column to remove water vapor from the output air before sending it into the ionization chamber. Using the mass-flow controller, the

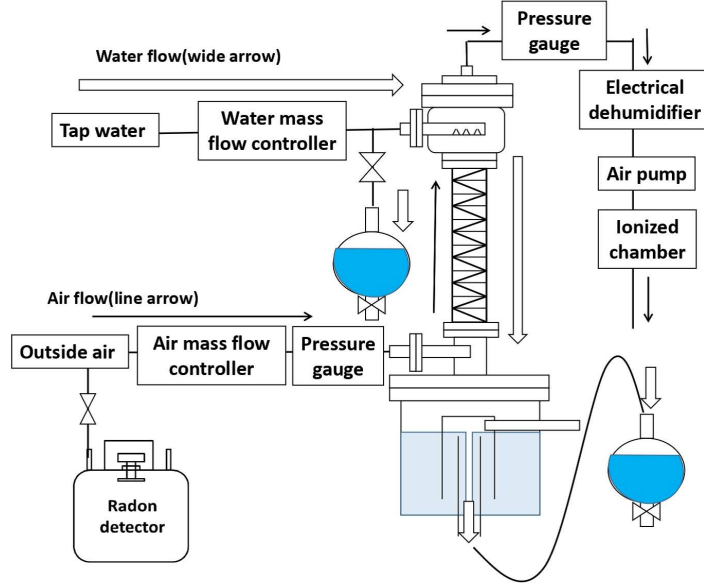


Figure 4: Schematic diagram of the calibration setup. Thin arrows show the direction of the air flow, while wide arrows show the direction of the water flow.

water flow rate was maintained at either $F_w = 4.0$ L/min or $F_w = 3.58$ L/min; which are flow rates used in the Super-K measurements described in Section 5.

Calibrations were performed as follows. First, tap water and purge air are supplied to the extraction column. After filling the buffer tank with the degassed water, we controlled their flow rates to maintain a constant water level in the PVC vessel (1st layer in Fig. 3). We then sampled the tap water and the Rn-degassed water at the same time using shake flasks. Note that when we found air bubbles on the inner surface of the shake flasks they were carefully removed in order to avoid Rn exchange between the sampling water and the air-bubbles. During the extraction process, the Rn concentrations in the purge air and output air were monitored using the 70 L Rn detector and the ionization chamber. Finally, the Rn extraction efficiency was determined according to Eq. (1).

The sources of systematic uncertainties in the calibration measurements are summarized in Table 1 and are primarily based on estimations from the technical specifications of the measurement devices. Measurements of the same sampling vials used in calibration found fluctuations in the Rn concentration of $\pm 7.5\%$ [54], which have been attributed to potential air leaks. If we assume that air leaks occurred during our measurements, the Rn concentration in the water may decrease, resulting in an erroneously low measured value. This would lead to an erroneously high extraction efficiency. In order to compensate for such problems, we take the value of these fluctuations as a systematic uncertainty. Additional systematic uncertainties are taken on the water flow rate stability, $\pm 2.0\%$, and the stability of the air flow rate, which is also $\pm 2.0\%$.

In total, we performed 6 (11) calibrations with the water flow rate set to $F_w = 4.0$ L/min ($F_w = 3.58$ L/min), as shown in Fig. 5. The measured extraction efficiencies are summarized in Table 2. Combining the first term with the second term in Eq. (2), we obtain the value of

Table 1: Systematic uncertainties in the calibration of the extraction efficiency. The second column shows typical values measured during the calibration procedure described in the text.

Systematic uncertainty	Typical value	Estimated uncertainty
Ionization chamber	8–12 Bq/L	$\pm 5.0\%$
70 L Rn detector [38]	0.01 Bq/L	$\pm 6.8\%$
Liquid scintillation counter	7–9 Bq/L or 2–3 Bq/L	$\pm 10.0\%$
Air leaks in sampling vials	–	$\pm 7.5\%$
Water flow rate	3.58 L/min or 4.0 L/min	$\pm 2.0\%$
Air flow rate	2.0 L/min	$\pm 2.0\%$

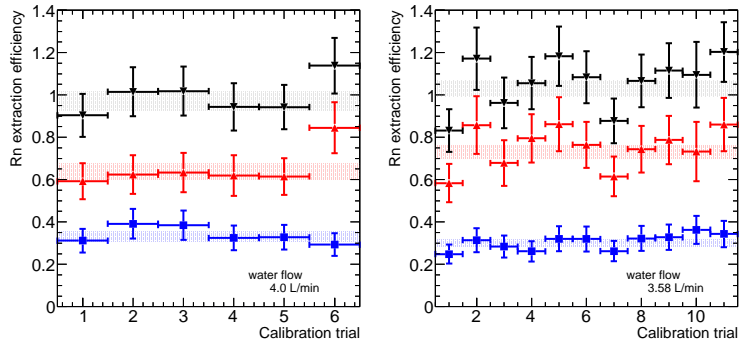


Figure 5: Efficiencies of the Rn extraction from the calibration measurements. The left figure shows the results for the water flow rate of 4 L/min and the right figure shows results for 3.58 L/min. Blue squares (red upward-pointing triangles) show the first (second) term defined in Eq. (2), and black downward-pointing triangles show their sum. Shaded bands show the total uncertainties for each term.

the sum to be 0.97 ± 0.05 (1.03 ± 0.04) for $F_w = 4.0$ L/min ($F_w = 3.58$ L/min). Both values are consistent with 1.0. This result demonstrates that the total radioactivity before and after extraction is conserved to within the measurement uncertainty.

To understand the stability of the extraction efficiency, we performed additional calibrations at a constant water flow of $F_w = 4.0$ L/min ($F_w = 3.58$ L/min) while changing the air flow from 1.6 L/min to 4.4 L/min (from 1.65 to 2.35 L/min). The ratio of the air and water flow rates varies between 0.4 and 1.1 (between 0.45 and 0.65). Fig. 6 shows the dependence of the extraction efficiency on this ratio. There is no correlation as summarized in Table 3.

3.2. Experimental setup and a method for radon concentration measurements

Charcoal efficiently absorbs various impurities [55] and is widely used to trap Rn from several gases [14, 40, 50, 56–59]. It has almost 100% trapping efficiency below -60°C and the trapped Rn can be removed with $\sim 100\%$ efficiency by heating the charcoal upto $+120^\circ\text{C}$ [60]. In order to take an advantage these properties, we designed a simple trap using a charcoal-filled 1/2 inch U-shaped electro-polished stainless steel pipe. The trap was filled with 12.5 g of charcoal (DIASORB G4-8, produced by Calgon Carbon Japan KK). This charcoal has also been used in previous studies [59]. When trapping Rn, the U-shaped pipe is placed in a refrigerated ethanol

Table 2: Summary of the measured extraction efficiencies with a constant air flow rate of $F_a = 2.0$ [L/min]. The first and the second terms are defined in Eq. (2).

F_w [L/min]	F_a [L/min]	First term	Second term	Total
4.00	2.0	0.33 ± 0.02	0.64 ± 0.04	0.97 ± 0.05
3.58	2.0	0.30 ± 0.02	0.73 ± 0.03	1.03 ± 0.04

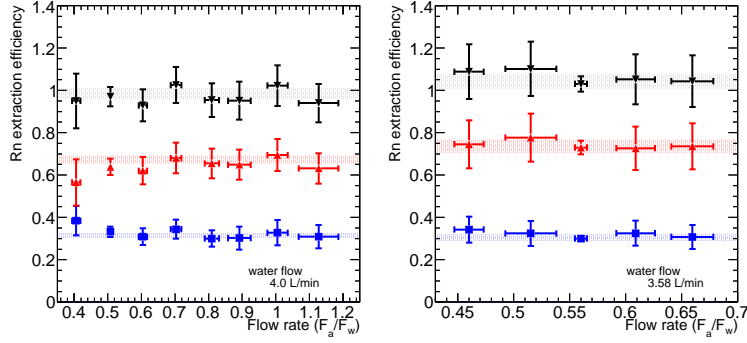


Figure 6: Dependence of the Rn extraction efficiency on the air flow rate. The water flow was fixed at 4.0 L/min for the left figure and 3.58 L/min for the right figure, while the air-flow rate was changed from 1.6 L/min to 4.4 L/min (from 1.65 L/min to 2.35 L/min). In the right panel, the third value is calculated by taking average of 11 measurements shown in Fig. 5. Other values are calculated by using the result from one measurement. Colored markers have the same definitions as in Fig. 5.

Table 3: Air flow rate dependence of the extraction efficiency. The first and the second terms are defined in Eq. (2).

F_w [L/min]	F_a [L/min]	First term	Second term	Total
4.00	1.6–4.4	0.31 ± 0.01	0.67 ± 0.02	0.98 ± 0.02
3.58	1.65–2.35	0.31 ± 0.01	0.73 ± 0.03	1.04 ± 0.03

bath. To release Rn from the trap, the U-shaped pipe is removed from the bath and heated with a band heater.

Fig. 7 shows a schematic diagram of the entire Rn measurement system. It consists of a water pump (Iwaki Co. Ltd., MDG-R15T100), a water mass-flow controller (TOFLO Corp., FLC620), a temperature sensor (TOFLO Corp., CF-SCMT, PTM-23), the Rn extraction system described in Section 3, two pressure gauges (Naganokeiki Co. Ltd., ZT67), an electrical dehumidifier (KELK, DH-209C), three copper wool traps for further water removal, the charcoal trap, a dew-point meter (VAISALA, DMT340), an air mass-flow controller (HORIBA STEC, Z512), an air-circulation pump, and the 80 L Rn detectors [50, 51]. We used three Rn detectors to conduct three measurements in parallel and they are identical.

A water sample can be supplied from the Super-K tank, from its pure water supply line, or from the return line to the water purification system. We used commercially-available G1-grade high-purity air (impurity < 0.1 ppm) as the purge gas to minimize intrinsic Rn backgrounds. It is important to remove water from the air before both the charcoal trap and the Rn detector, as their efficiencies depend on the humidity [61]. The electrical dehumidifier and three copper wool traps are used for this purpose. Each copper wool trap is a 3/4 inch U-shaped pipe filled with 12.5 g of φ 80 μm copper wool (Nippon Steel Wool Cp., Ltd.). We placed these in an ethanol bath kept below -80°C . Note that Rn is not captured by the copper wool². Further, we installed 0.4 μm mesh filters (Pall Corp., CNF1004USG6) before and after the Rn trap to prevent pieces of charcoal from escaping into the measurement system. We used 1/2 inch nylon tubes (NITAA, MOORE N2) to sample the water. Other system components are made of electro-polished stainless steel (NISSHO Astec Co., Ltd., MGS-EP SUS316L) and all joints are connected by VCR[®] gaskets to minimize Rn emanation and possible air leaks, both of which can affect backgrounds in the measurement.

There are three steps to measure the Rn concentration in water. First, Rn is extracted from the water using the extraction column described before and is concentrated in the chilled charcoal trap (concentration process). In the next step, the Rn gas is released from the trap and transferred to the Rn detector (transfer process). Finally, the Rn concentration is measured with the 80 L detector (measurement process).

Before any measurement, the entire system except for the water lines, the extraction column, and the charcoal trap is first evacuated down to $< 1.0 \times 10^{-4}$ Pa. The air leak rate of the system was measured to be less than 10^{-10} Pa \cdot m³/sec using a helium leak detector (HELIOT 712D2, produced by ULVAC Equipment Sales Inc). The trap is then heated to $+200^\circ\text{C}$ for about one hour to completely remove any residual Rn. Afterwards the system is filled to atmospheric pressure with commercially-available G1-grade high purity air (impurity concentration < 0.1 ppm) and the trap is cooled with a refrigerator. During the concentration process, we set the water sampling rate to 3.58 L/min or 4.0 L/min and set the flow rate of the purge air to 2.0 L/min. After the water level and the air pressure in the extraction column stabilize, valves before and after the charcoal trap were opened, as shown in Fig. 7. Sampling and concentration periods varied from 0.5 hours to 18 hours, depending upon the expected Rn concentration of a given measurement.

After the concentration process, the valves before and after the charcoal trap were closed and the water sampling was stopped. During the transfer process, we heated the trap to $+200^\circ\text{C}$ and then opened the valves again to supply pure air at 1.0 L/min in order to fill the Rn detector with

²We evaluated the capture rate of Rn on the copper wool with another calibration set up. We confirmed that the Rn concentration did not decrease when the pure air was circulated through the cooled copper trap in the closed set up. Thereby, the capture of Rn on the copper wool is negligible in the analysis described in Section 3.3.

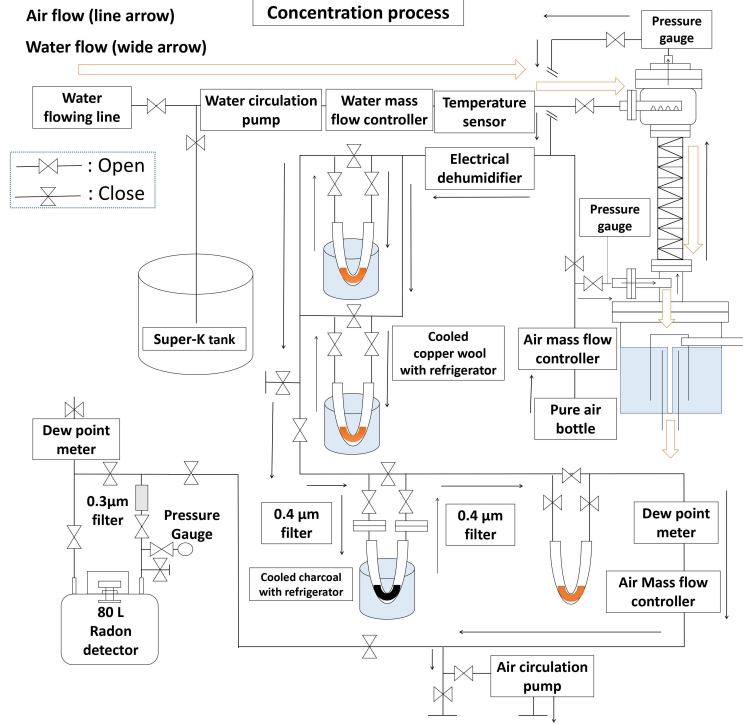


Figure 7: Schematic diagram of the setup for the Rn concentration process. The thin arrows show the direction of the purge air flow, while thick arrows show the direction of the sampled (and degassed) water.

the accumulated Rn. The entrance valve was closed after the Rn detector reached atmospheric pressure. After these procedures measurements were started and performed typically for 20 days in order to determine the shape of the Rn decay curve.

3.3. Analysis method

Since Rn decays with a constant half-life its initial concentration at the start of the measurement can be derived from the measured decay curve. Fig. 8 shows an example of the measured concentration as a function of time. The data is fitted with the following function:

$$C(t) = Ae^{-\lambda t} + B_{\text{detector}} (1 - e^{-\lambda t}), \quad (3)$$

where t [day], $C(t)$ [mBq/m³], λ [day⁻¹], A [mBq/m³], and B_{detector} [mBq/m³] are the elapsed time since the start of the measurement, the Rn decay constant ($\lambda = \ln 2 / \{3.82 \text{ day}\} = 0.181 \text{ day}^{-1}$), the Rn concentration at time t , the initial Rn concentration, and the background due to the activity of ²²⁶Rn in the Rn detector, respectively. These parameters are listed in Table 4. Note that in a previous publication [50] we found B_{detector} to be $0.33 \pm 0.07 \text{ mBq/m}^3$ for a particular 80 L detector. After the actual measurements described in Section 5, we have evaluated the background of three Rn detectors used in the measurement system. The backgrounds were measured by closing the Rn detector. We used about 89 days data taken from November 1st 2015 to January 29th

Table 4: Summary of the parameters used to calculate the Rn concentration in water.

Parameter	Value	Unit	Definition
t		day	Elapsed time since the start of measurement
$C(t)$		mBq/m ³	Rn concentration measured by the Rn detector at time t
A		mBq/m ³	Rn concentration at the start of measurement
λ	$\ln 2/3.82$	day ⁻¹	²²² Rn decay constant
B_{detector}	1.24 ± 0.10	mBq/m ³	Background of 80 L Rn detector No. 1
	0.24 ± 0.04		Background of 80 L Rn detector No. 2
	0.27 ± 0.04		Background of 80 L Rn detector No. 3
t_{con}		hour	Duration of the concentration process
t_{total}		hour	Combined duration of the concentration and transfer processes
F_a (F_w)		L/min	Purge air (sampled water) flow rate
C_{PAD}		mBq/m ³	Rn concentration in purge air after degassing
V_{det}	0.080	m ³	Volume of the 80 L Rn detector
V_{purge}	$F_a \times t_{\text{con}}$	m ³	Purge air volume
β_{corr}	$\exp(-\lambda t_{\text{total}})$		Correction factor due to Rn decay during concentration and transfer processes
$\varepsilon_{\text{mixing}}$	See Table 2		Extraction column Rn extraction efficiency
$\varepsilon_{\text{trap}}$	0.99 ± 0.01		Charcoal trap trapping efficiency
ε_{rel}	0.99 ± 0.01		Charcoal trap release efficiency

2016. Each backgrounds are 1.24 ± 0.10 mBq/m³, 0.27 ± 0.04 mBq/m³, and 0.23 ± 0.04 mBq/m³, respectively. The first detector has the larger background than that of others. This is because this detector was reused from the previous Rn detector by replacing its top flange and by performing the electropolish to its inner surface. Due to such additional production processes, it was slightly contaminated.

In the fitting process of the analysis, the parameter of the detector background, B_{detector} , is fitted by limiting its value within $\pm 3\sigma$ of the statistical uncertainty of each average background rate listed in Table 4.

After obtaining A from the fit, we derived the Rn concentration in the air. We obtained the initial total radioactivity in the detector as $A \times V_{\text{det}}$, where $V_{\text{det}} = 0.080$ m³ is the total volume of the Rn detector. On the other hand, the total radioactivity in the purge air after extracting is given by $C_{\text{PAD}} V_{\text{purging}}$, where C_{PAD} is the Rn concentration in the purge air after the extraction and $V_{\text{purging}} = F_a \times t_{\text{con}}$ is the total volume of the purge air that passes through the charcoal trap during the concentration process (F_a is the flow rate of the purge air). Since the initial total radioactivity AV_{det} should be the same as $C_{\text{PAD}} V_{\text{purge}}$, we obtain the Rn concentration in the purge air after degassing as $C_{\text{PAD}} = AV_{\text{det}}/V_{\text{purge}}$. Here, the efficiencies of Rn trapping ($\varepsilon_{\text{trap}}$) and release (ε_{rel}) are assumed to be 0.99 ± 0.01 , since the former (latter) reaches almost 100% when the trap is cooled down to -60°C (baked at more than $+120^\circ\text{C}$) [60], as mentioned above. Then, we derived the Rn concentration in the sampled water by dividing C_{PAD} by the Rn extraction efficiency. Since the concentration and transfer processes take hours, Rn decay during the entire measurement must also be considered. We used the correction term $\beta_{\text{corr}} = \exp(-\lambda t_{\text{total}})$ for this analysis, where t_{total} is the total time required for both the concentration and transfer processes.

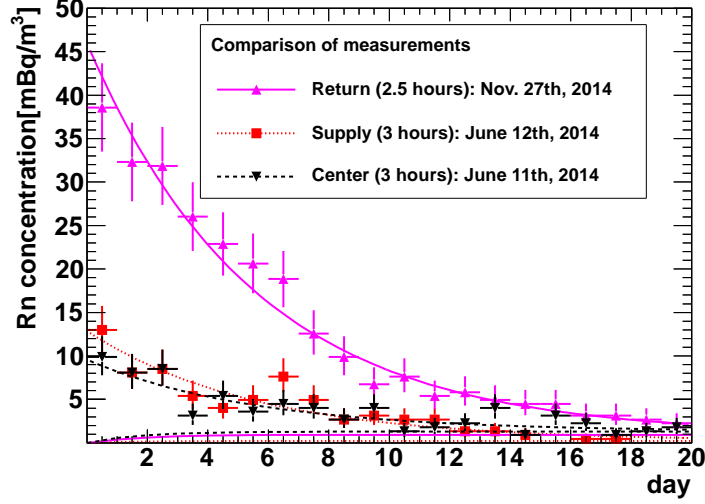


Figure 8: Measurement results. Super-K detector supply water Rn concentration (red), that of its return water (pink), and water from its center (black). The horizontal axis shows the elapsed time and the vertical axis shows the Rn concentration as measured with the 80 L Rn detector. The fitted curves are defined by Eq. (3).

Finally, we obtain the Rn concentration of the sampled water (C_{sample}) from

$$C_{\text{sample}} = \frac{A}{\beta_{\text{corr}}} \times \frac{V_{\text{det}}}{V_{\text{purge}}} \times \frac{F_a}{\epsilon_{\text{mixing}} F_w} \times \frac{1}{\epsilon_{\text{trap}} \epsilon_{\text{rel}}}, \quad (4)$$

where the parameters used in this equation are listed in Table 4.

4. Backgrounds and systematic uncertainties

Although all materials and system components were carefully selected, a Rn background still exists due to air leaks and emanation from contaminants on the inner surfaces of the setup. To evaluate this background we performed several dedicated measurements. Note that this background, which we define as B_{system} , is to be distinguished from the intrinsic background of the Rn detector itself, defined as B_{detector} in Eq. (3). Possible background sources are (A) residual Rn in the G1-grade pure air, (B) Rn emanation from the inner surface of the air flow line, including the electrical dehumidifier and copper wool traps, (C) emanation from the inner surface of the extraction column, including the PVC acrylic vessel, (D) emanation from the charcoal, and (E) emanation from the components of the water sampling line, such as the nylon tube and the water pump. The total background in the system is given by $B_{\text{system}} = B_{\text{air-line}} + B_{\text{column}} + B_{\text{water-line}}$, where $B_{\text{air-line}}$ is the backgrounds (A), (B) and (D), B_{column} is the background from (C), and $B_{\text{water-line}}$ is that from (E).

4.1. Backgrounds from the air lines

In order to evaluate $B_{\text{air-line}}$, we performed measurements after bypassing the extraction column. The valves before and after the extraction column were closed and air was supplied directly

Table 5: Summary of background evaluated in Section 4. As described in the main text, the total background is proportional to the total duration of measurement processes. Therefore, the hourly background is listed in the second column. In addition to this, the Rn concentration of background is also calculated by normalizing total amount of used air (sampled water) as listed in the third column.

Background	mBq/hour	mBq/m ³
$B_{\text{air-line}}$	0.013 ± 0.002	0.11 ± 0.01
$B_{\text{column}} + B_{\text{water-line}}$	0.143 ± 0.027	0.67 ± 0.12

to the dehumidifier, copper wool traps, and the charcoal trap during the concentration process. We then performed the transfer and measurement processes and obtained $B_{\text{air-line}}$ from

$$B_{\text{air-line}} = \frac{A}{\beta_{\text{corr}}} \times \frac{V_{\text{det}}}{V_{\text{purge}}} \times \frac{1}{\varepsilon_{\text{trap}} \varepsilon_{\text{rel}}}, \quad (5)$$

where A , β_{corr} , V_{det} , V_{purge} , ε_{rel} and $\varepsilon_{\text{trap}}$ are listed in Table 4.

We performed four measurements for different durations of the concentration process (19, 21.5, 22, and 24 hours). During the concentration process of these measurements, we cooled the charcoal trap down to -70°C as usual. After this process, we baked the charcoal trap to release the absorbed Rn and transferred the accumulated Rn to the Rn detector as usual. These measurements give the total background caused by intrinsic background from purified air, Rn emanation from the charcoal, and from the system itself. Using Eq. (5) we estimated the backgrounds from the air line to be $B_{\text{air-line}} = 0.013 \pm 0.002$ mBq/hour, which is also listed in Table 5. Since this background is proportional to some extent to the total duration of the concentration process (t_{con}), this estimated background can be normalized by the total amount of air used and can be expressed as $B_{\text{air-line}} = 0.11 \pm 0.02$ mBq/m³. Accordingly, the intrinsic Rn concentration in the G1-grade pure air is below this level.

4.2. Backgrounds from the extraction column and water lines

In order to determine $B_{\text{mixer}} + B_{\text{water-line}}$, a closed-loop running [40, 44], where Rn-degassed water is sent to the extraction column repeatedly, is used. From Eq. (2), the Rn concentration in the degassed water after one extraction cycle is given by $C_w = C_{w,0}(1 - \varepsilon_{\text{mixing}}) = C_{w,0}p$, where C_w , $C_{w,0}$, and $\varepsilon_{\text{mixing}}$ are as defined in Section 3.3. Here p is $(1 - \varepsilon_{\text{mixing}})$. The Rn concentration in the sampling water just before the extraction column is

$$C_{w,0} = C_{\text{sample}} + B_{\text{water-line}}, \quad (6)$$

where C_{sample} is the concentration in the sampled water. The concentration in the Rn-degassed water is then

$$C_{\text{degassed}} = p(C_{w,0} + B_{\text{column}}) = p(C_{\text{sample}} + B_{\text{water-line}} + B_{\text{column}}). \quad (7)$$

After performing the extracting processes n times (i.e., after looping through the system n times), the Rn concentration in the degassed water ($C_{n\text{-looped}}$) can be written as

$$C_{n\text{-looped}} = p^n C_{\text{sample}} + \frac{1 - p^n}{1 - p} (B_{\text{water-line}} + B_{\text{column}}). \quad (8)$$

Table 6: Summary of the systematic uncertainties for the measurement system.

Source	Systematic uncertainty
Rn extraction efficiency (ϵ_{mixing})	Table 1
80 L Rn detector calibration	$\pm 5.7\%$ [50]
Difference among three 80 L Rn detectors	$\pm 10.0\%$ [50, 51]
Water flow rate (F_w)	$\pm 2.0\%$
Air flow rate (F_a)	$\pm 2.0\%$
Rn trapping efficiency (ϵ_{trap})	$\pm 1.0\%$
Rn release efficiency (ϵ_{rel})	$\pm 1.0\%$

Therefore, after a large number of mixings, the concentration, $C_{\text{closed-loop}}$, reaches an equilibrium that is determined by the background and the extraction efficiency:

$$C_{\text{closed-loop}} = \frac{1}{1-p} (B_{\text{water-line}} + B_{\text{column}}). \quad (9)$$

In order to prepare water for the closed-loop running, we conducted this operation for more than 6 hours ($n > 50$) and measured the Rn concentration following the method described in the previous section. The result is $C_{\text{closed-loop}} = 0.196 \pm 0.028$ mBq/hour for a water flow rate $F_w = 3.58$ L/min. Thus, we obtain the background as $B_{\text{water-line}} + B_{\text{column}} = 0.143 \pm 0.027$ mBq/hour as listed in Table 5. We use this value in the measurements below. Moreover, the estimated background is normalized by the total amount of sampled water and expressed as $B_{\text{water-line}} + B_{\text{column}} = 0.67 \pm 0.12$ mBq/m³, which corresponds to the total background when 1 m³ of water is sampled (about 5 hours for 3.58 L/min, about 4 hours for 4.0 L/min.). Since the inner surface of the extraction column has been electro-polished, the Rn emanation rate from this part of the system is expected to be low. In contrast, we expect the background from the PVC vessel to be relatively high and it may be the main background source. Systematic uncertainties for measurements with this system are summarized in Table 6.

5. Radon concentration measurements

5.1. Supply water

Since Rn contamination in the Super-K supply water can be a potentially dangerous source of backgrounds, monitoring its concentration is essential to understand those backgrounds and the stability of the detector's response to them. Measurements of the Rn concentration in the supply water were done using a sampling port located after the last stage of the water circulation system (after HE4 in Fig. 1). Using data taken from June 2014 to October 2015, the Rn concentration in the supply water was found to be stable at $C_{\text{Supply}} = 1.74 \pm 0.14$ mBq/m³ as shown in Fig. 9.

5.2. ID bottom

Since water is supplied to the Super-K tank through ID via inlets at its bottom (Fig. 2), measurements of the Rn concentration there should track those of the supply water itself. Water is sampled from this region by inserting a 1/2-inch nylon tube from the top of the detector at

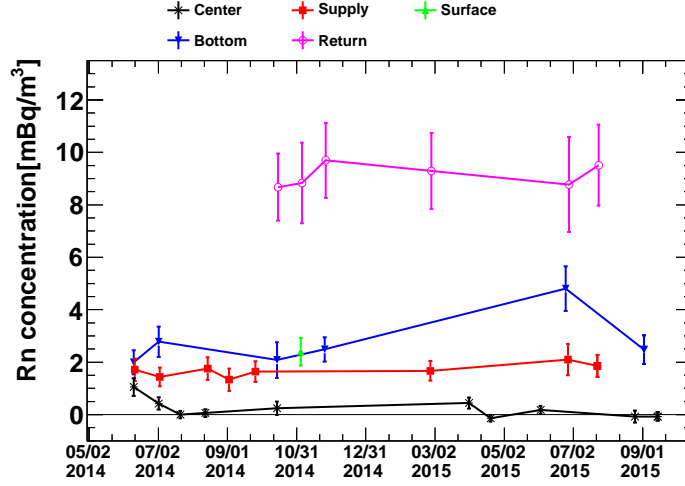


Figure 9: Measured Rn concentrations in various Super-K water samples as a function of time. The black crosses, red squares, green upward-pointing triangles, blue downward-pointing triangles, and pink circles show results for the center region, the supply water, water sampled from the surface of the tank water, the bottom region, and the return water, respectively.

$(x, y, z) = (+0.353, -0.707)$ m and lowering it to $z = -12.000$ m. This location is also used to calibrate the detector near its energy threshold [16, 62] and therefore Rn backgrounds in this area are of particular interest. We performed several measurements as shown in Fig. 9 and found $C_{\text{ID-bottom}} = 2.63 \pm 0.22$ mBq/m³. Note that this is a higher concentration than that of the supply water, the implications of which are discussed in the next section.

5.3. Center of the Super-K tank

Typically the center region of the Super-K detector is the most radio-pure, since it is far from the detector walls, water inputs and returns. As a result, it is the best candidate for studying very low energy solar neutrino interactions and consequently it is essential to understand backgrounds from any residual Rn daughters therein. Accordingly, water was sampled at the same (x, y) location as discussed above, but at $z = +0.400$ m in order to study the center of the detector. The results are shown in the thick black line of Fig. 9. As expected, the Rn concentration in this region is quite low, often consistent with zero within the measurement errors. The measurement shows a negative central value, which has been attributed to fluctuations of the background. We note that in these cases the upper limit on the concentration is $C_{\text{Center}} < 0.23$ mBq/m³ (95% C.L.).

5.4. Return water

The SK-IV water circulation system pumps water out of the tank for re-purification via outlets placed at the top and bottom of the detector (Fig. 2). This return water is a mixture of water from the OD surface, the OD barrel (i.e. the OD outlet shown in the right panel of Fig. 2), the ID top, and the OD bottom. The corresponding flow rates are listed in Table 7. Since a significant fraction of the water is from the OD, which is surrounded by Rn sources, including the tank

Table 7: Super-K water flow. As shown in Fig. 2, the return water is a mixture of the water from the OD surface, ID+OD top, and OD bottom regions.

Position	Water flow rate [ton/hour]
OD surface	12
ID+OD top	36
OD bottom	12
Return	60

lining and cavern rock, it is important to measure the return water’s Rn concentration to identify potential background sources in the ID.

Return water was sampled from a port located just after the pump to send water from the tank back to the circulation system (return pump in Fig. 1). The measured Rn concentration was $C_{\text{Return}} = 9.06 \pm 0.58 \text{ mBq/m}^3$. It is clear that water that has passed through PMTs and the detector structure has higher concentration than that of the supply water. Comparison of the return and supply concentrations indicates that the water circulation system’s total Rn removal efficiency is 0.81 ± 0.08 .

5.5. Measurement verification

As shown in Fig. 9, the Rn concentrations in various water samples have been stable to within their measurement uncertainties. Assuming that the concentrations are constant on the time scale of several hours, we can test the validity of the measurement as follows. If the total amount of Rn is proportional to the total amount of sampled water, the accumulated Rn (A/β_{corr}) should be a linear function of the total sampled water volume (integrated flow). The slope of this function corresponds to the Rn concentration in the sampled water. Fig. 10 shows the accumulated Rn concentration as a function of the total amount of sampled water and displays the expected linear relationship.

By fitting the slope, the Rn concentrations in the sampled water can be derived from the following equation, independent of Eq. (4):

$$C_{\text{sampled}} = \frac{V_{\text{det}} \times \text{slope}}{\epsilon_{\text{trap}} \epsilon_{\text{rel}} \epsilon_{\text{mixing}}}. \quad (10)$$

The Rn concentrations obtained with this method are summarized in Table 8 and compared with those from Eq. (4) after subtracting the backgrounds described in Section 4. The table also lists the χ^2 values and corresponding p -values from the fits. Regarding the latter, we note that with the exception of the center region, which has suffered fluctuations in the background, each fit is compatible with the hypothesized linear relationship. Further, the consistency of results across measurement methods indicates that the observed Rn concentrations in the Super-K water are accurate at the mBq/m^3 level.

5.6. Comparison with past measurements

Table 9 shows a comparison of the Rn concentrations in the supply and return water measured in this study as well as previous measurements [13, 38, 48]. The Rn concentrations in the supply water and return water during SK-IV are higher than those measured during SK-I.

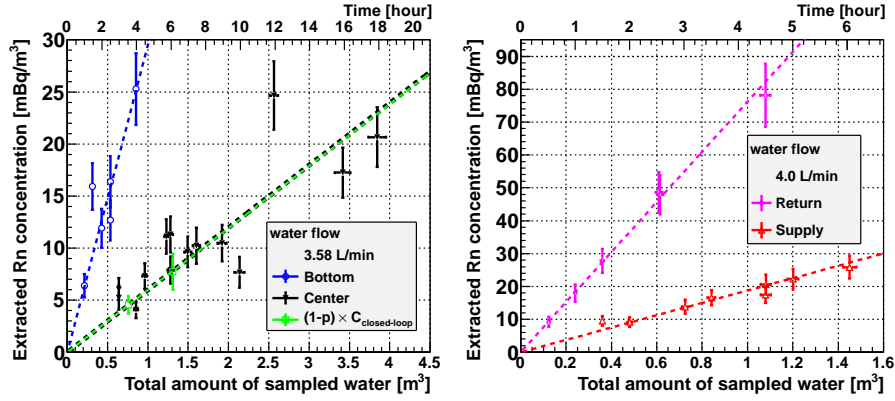


Figure 10: Relationship between the extracted Rn concentration and the total amount of sampled water. The vertical axis shows the extracted Rn concentration after correcting for the time factor β_{corr} and the lower (upper) horizontal axis shows the total amount of sampled water (total duration of the concentration process, t_{con} in Table 4). The left figure shows results for water sampled from the tank, as well as for the closed-loop water, at a flow rate $F_w = 3.58$ L/min. Similarly, results for the supply and return lines at a flow rate of $F_w = 4.0$ L/min are shown in the right figure.

Table 8: Summary of the measurement results obtained from the methods of Eq. (4) and Eq. (10), as well as the χ^2 per degree of freedom and corresponding p -value from the latter.

Sampled water	Eq. (4) [mBq/m ³]	Eq. (10) [mBq/m ³]	$\chi^2/\text{d.o.f}$	p -value
Supply	1.74 ± 0.14	1.64 ± 0.50	5.053/7	0.653
ID bottom	2.63 ± 0.22	2.63 ± 0.30	11.68/5	0.039
Center	< 0.23 (95% C.L.)	< 0.26 (95% C.L.)	40.76/13	0.010
Return	9.06 ± 0.58	8.71 ± 1.96	0.37/5	0.996
$(1-p)C_{\text{closed-loop}}$ $= B_{\text{air-line}} + B_{\text{column}}$	0.67 ± 0.12	0.67 ± 0.10	–	–

Table 9: Summary of the measured Rn concentration in supply water and return water.

Sampling water	Phase	Result [mBq/m ³]	Method
Supply	Beginning of SK-I	< 3.2	70 L Rn detector w/ plastic ball [13, 38]
Supply	End of SK-I	0.4 ± 0.2	700 L Rn detector w/ membrane [14, 48]
Supply	SK-IV (This study)	1.74 ± 0.14	80 L Rn detector w/ extraction column
Return	Beginning of SK-I	< 5.0	70 L Rn detector w/ plastic ball [13, 38]
Return	End of SK-I	< 2.0	700 L Rn detector w/ membrane [14, 48]
Return	SK-IV (This study)	9.06 ± 0.58	80 L Rn detector w/ extraction column

Table 10: Summary of the measured Rn concentration in the tank water.

Detector position	Phase	Result [mBq/m ³]	Method
Tank water	Beginning of SK-I	< 5.7	70 L Rn detector w/ plastic ball [13, 38]
$0 \leq z \leq 10$ m	Beginning of SK-I	< 1.4	Rn injection calibration [13]
$z = -6$ m	Beginning of SK-I	3.0	Rn injection calibration [13]
$z = -11$ m	Beginning of SK-I	5.0	Rn injection calibration [13]
$z = +0.4$ m	SK-IV (This study)	< 0.23	80 L Rn detector w/ extraction column
$z = -12$ m	SK-IV (This study)	2.63 ± 0.22	80 L Rn detector w/ extraction column

However, the Rn reduction efficiency of the former (0.81 ± 0.08) is comparable to that of the latter (~ 0.80). Accordingly, the higher Rn concentration in the SK-IV return water resulted in the higher concentration in the supply water.

In the previous study, the Rn concentrations in the tank were estimated using a Rn injection calibration method [13]. Table 10 shows a comparison of Rn concentrations in the tank water. For the region between ± 0 m and +10 m an upper limit of < 1.4 mBq/m³ was obtained during SK-I. Further, the estimated Rn concentration at $z = -6$ m ($z = -11$ m) was 3.0 mBq/m³ (5.0 mBq/m³). On the other hand, the measured Rn concentrations with system used in this manuscript are < 0.23 mBq/m³ in the center region ($z = +0.4$ m) and 2.63 ± 0.22 mBq/m³ in the bottom region ($z = -12$ m). Based on those results, the measurement technique presented in the article has improved the measurement sensitivity to the Rn concentration in purified water comparing with the past techniques.

The results are summarized in Table 10 and suggest that the Rn concentrations in the center region and the bottom region, which are used for solar neutrino analysis, are clearly lower in SK-IV. Therefore, we conclude that we have successfully reduced the Rn in the both regions by optimizing both the supply water temperature and the water circulation rate. On the other hand, this optimization results in higher Rn concentrations in the supply water and in the return water, indicating that the dominant sources of Rn are in the Super-K tank itself and not in the water system or buffer gas (see below).

Further discussion related to Rn sources in the water tank and the observed background rate caused by Rn daughters in the Super-K solar neutrino analysis will be presented in a subsequent

publication.

6. Other OD Measurements

The bottom region of OD may also have a large Rn concentration because dust from the detector volume may settle and accumulate there. Although measurements of its water may provide hints at possible Rn sources in the tank, it is impossible to directly sample water from this region.

However, the Rn concentration in the OD bottom water can be indirectly estimated since part of the return water is taken from this region (see Table 7). The estimation proceeds via the following equation:

$$C_{\text{OD-bottom}} = \frac{C_{\text{return}}F_{\text{return}} - (C_{\text{OD-surface}}F_{\text{OD-surface}} + C_{\text{ID-top}}F_{\text{ID-top}} + C_{\text{OD-barrel}}F_{\text{OD-barrel}})}{F_{\text{OD-bottom}}}, \quad (11)$$

where variables beginning with C represent the Rn concentrations of each water sample, and similarly, those with F represent the flow rates. In order to obtain $C_{\text{OD-barrel}}$ for this estimate, we sampled water from the barrel region of the OD barrel by inserting a sampling tube at $(x, y, z) = (+17.321, -3.535, +17.000)$ m on November 6, 2014 and measured the Rn concentration of 3.48 ± 0.60 mBq/m³. Although the water tank in the top region of ID has not been measured directly, we estimate its Rn concentration to be equal to that of the ID center, i.e., $C_{\text{ID-top}} \sim C_{\text{center}}$, based on Super-K low energy background data [9, 63, 64]. Using these measurements and assumptions, we estimate the concentration in the OD bottom to be $C_{\text{OD-bottom}} = 33.97 \pm 3.30$ mBq/m³. Note that this region is expected to be the least radio-pure region in the Super-K tank.

In the Super-K tank there is a buffer gas layer between the surface of the OD water and the top of the tank [14]. In previous publications [50], we have concluded that Rn contamination from the Super-K tank itself is the dominant source of Rn in this buffer gas. This suggests that Rn in the buffer gas, whose concentration was measured to be 28.8 ± 1.7 mBq/m³, dissolves into the OD top water. In order to confirm this Rn contamination directly, we measured the Rn concentration at depth of 20 cm below the surface of the tank water by inserting a nylon tube into the calibration hole at $(x, y) = (-0.950, -1.064)$ m. The resulting Rn concentration was 2.51 ± 0.47 mBq/m³, indicating that the surface water is not the main source of Rn in the buffer gas and suggesting further the detector structure is the primary Rn source.

7. Conclusion and future prospects

We have developed a new technique for measuring ultra-low Rn concentrations in purified water. For this purpose, we developed and calibrated an extraction column to extract Rn from water with extraction efficiencies of 0.64 ± 0.03 for a water flow rate of $F_w = 4.0$ L/min and 0.73 ± 0.04 for $F_w = 3.58$ L/min when $F_a = 2.0$ L/min. For fixed values of the water flow, we additionally found the efficiency has no dependence on the air flow rate.

Combining the extraction column with an existing 80 L Rn detector we have constructed a new Rn measurement system for the Super-K water. Using this system, we measured the Rn concentration at several places in the Super-K tank and the water system with a background of 0.143 ± 0.027 mBq/hour, which corresponds to 0.67 ± 0.12 mBq/m³ when 1 m³ of water

is sampled. During the period from June 2014 to October 2015, the Rn concentrations were stable at 1.74 ± 0.14 mBq/m³ in the supply water, < 0.23 mBq/m³ (95% C.L.) in the ID center, 2.63 ± 0.22 mBq/m³ at the bottom of the ID, and 9.06 ± 0.58 mBq/m³ in the return water. Comparing the supply water with the return water, we conclude that the dominant Rn sources are in the Super-K tank rather than in the water system or buffer gas.

The method developed in this study will enable other solar neutrino detectors, such as SK-Gd and Hyper-Kamiokande [65], to monitor the Rn concentrations in their purified water in detail.

Acknowledgements

The authors would like to thank the Super-Kamiokande collaboration for their help in conducting this study. Especially, we thank M. Miura who supported the scheduling to open the tank. We acknowledge the cooperation of the Kamioka Mining and Smelting Company. We would like to thank the reviewers for their thoughtful comments and careful review, which helped improve our manuscript. Y. N thanks M. Kanazawa for helping the work to assemble the measurement system at the experimental area of the Super-K. In addition, Y. N thanks N. Nozawa, T. Onoue, Y. Tamori, T. Higashi and T. Ushimaru for transporting air bottles. Y. N thanks K. Watanabe and H. Nagao who supported the calibration works. Y. N also thanks M. Ikeda, T. Yano, G. Pronost, S. Ito, K. Iwamoto, Y. Suda, A. Orii, R. Akutsu, D. Fukuda, C. Xu, K. Ito and Y. Sonoda who supported the water sampling work. This work is partially supported by the inter-university research program at ICRR. This work is partially supported by MEXT KAKENHI Grant Number 26104008, 17K17880, and 18H05536.

References

- [1] Ziro Maki, Masami Nakagawa, Shoichi Sakata, Remarks on the Unified Model of Elementary Particles, *Prog. Theor. Phys.* 28 (1962) 870.
- [2] B. Pontecorvo, Neutrino Experiments and the Problem of Conservation of Leptonic Charge, *Soviet Physics JETP* 26 (1968) 984–988.
- [3] S. Fukuda, et al., Solar ⁸B and hep Neutrino Measurements from 1258 Days of Super-Kamiokande Data, *Phys. Rev. Lett.* 86 (2001) 5651.
- [4] Q.R. Ahmad, et al., Measurement of the Rate of $\nu_e + d \rightarrow p + p + e^-$ Interactions Produced by ⁸B Solar Neutrinos at the Sudbury Neutrino Observatory, *Phys. Rev. Lett.* 87 (2001) 071301.
- [5] Q.R. Ahmad, et al., Direct Evidence for Neutrino Flavor Transformation from Neutral-Current Interactions in the Sudbury Neutrino Observatory, *Phys. Rev. Lett.* 89 (2002) 011301.
- [6] J. Hosaka, et al., Solar neutrino measurements in Super-Kamiokande-I, *Phys. Rev. D* 73 (2006) 112001.
- [7] J.P. Cravens, et al., Solar neutrino measurements in Super-Kamiokande-II, *Phys. Rev. D* 78 (2008) 032002.
- [8] K. Abe, et al., Solar neutrino results in Super-Kamiokande-III, *Phys. Rev. D* 83 (2011) 052010.
- [9] K. Abe, et al., Solar neutrino measurements in Super-Kamiokande-IV, *Phys. Rev. D* 94 (2016) 052010.
- [10] S.P. Mikheyev and A.Y. Smirnov, Resonance enhancement of oscillations in matter and solar neutrino spectroscopy, *Sov. J. Nucl. Phys.* 42 (1985) 913–917.
- [11] L. Wolfenstein, Neutrino oscillations in matter, *Phys. Rev. D* 17 (1978) 2369.
- [12] A. Renshaw, et al., First Indication of Terrestrial Matter Effects on Solar Neutrino Oscillation, *Phys. Rev. Lett.* 112 (2014) 091805.
- [13] Y. Takeuchi, et al., Measurement of radon concentrations at Super-Kamiokande, *Phys. Lett. B* 452 (1999) 418–424.
- [14] S. Fukuda, et al., The Super-Kamiokande detector, *Nucl. Instrum. Meth. Phys. Res. Sect. A* 501 (2003) 418–462.
- [15] S. Yamada, et al., Commissioning of the new electronics and online system for the Super-Kamiokande experiment, *IEEE Trans. Nucl. Sci.* 57 (2010) 428–432.
- [16] K. Abe, et al., Calibration of the Super-Kamiokande, *Nucl. Instrum. Meth. Phys. Res. Sect. A* 737 (2014) 253–272.
- [17] B. Aharmim, et al., Combined analysis of all three phases of solar neutrino data from the Sudbury Neutrino Observatory, *Phys. Rev. C* 88 (2013) 025501.

- [18] B.T. Cleveland, et al., Measurement of the Solar Electron Neutrino Flux with the Homestake Chlorine Detector, *Astrophys. J.* 496 (1998) 505–526.
- [19] J.N. Abdurashitov, et al., Measurement of the solar neutrino capture rate with gallium metal. III. Results for the 2002–2007 data-taking period, *Phys. Rev. C* 80 (2009) 015807.
- [20] M. Altmann, et al., Complete results for five years of GNO solar neutrino observations, *Phys. Lett. B* 616 (2005) 174–190.
- [21] K.S. Hirata, et al., Observation of ^8B solar neutrinos in the Kamiokande-II detector, *Phys. Rev. Lett.* 63 (1989) 16.
- [22] Y. Fukuda, et al., Solar Neutrino Data Covering Solar Cycle 22, *Phys. Rev. Lett.* 77 (1996) 1683.
- [23] B. Aharmim, et al., Electron energy spectra, fluxes, and day-night asymmetries of ^8B solar neutrinos from measurements with NaCl dissolved in the heavy-water detector at the Sudbury Neutrino Observatory, *Phys. Rev. C* 72 (2005) 055502.
- [24] B. Aharmim, et al., Measurement of the ν_e and total ^8B solar neutrino fluxes with the Sudbury Neutrino Observatory phase-III data set, *Phys. Rev. C* 87 (2013) 015502.
- [25] G. Bellini, et al., Measurement of the solar ^8B neutrino rate with a liquid scintillator target and 3 MeV energy threshold in the Borexino detector, *Phys. Rev. D* 82 (2010) 033006.
- [26] G. Bellini, et al., First Evidence of *pep* Solar Neutrinos by Direct Detection in Borexino, *Phys. Rev. Lett.* 108 (2012) 051302.
- [27] G. Bellini, et al., Final results of Borexino Phase-I on low-energy solar neutrino spectroscopy, *Phys. Rev. D* 89 (2014) 112007.
- [28] G. Bellini, et al., Neutrinos from the primary proton-proton fusion process in the Sun, *Nature* 512 (2014) 383–386.
- [29] M. Agostini, et al., Simultaneous precision spectroscopy of pp , ^7Be , and *pep* solar neutrinos with Borexino Phase-II, *Phys. Rev. D* 100 (2019) 082004.
- [30] S. Abe, et al., Measurement of the ^8B solar neutrino flux with the KamLAND liquid scintillator detector, *Phys. Rev. C* 84 (2011) 035804.
- [31] A. Gando, et al., ^7Be solar neutrino measurement with KamLAND, *Phys. Rev. C* 92 (2015) 055808.
- [32] P.C. de Holanda and A.Yu. Smirnov, Homestake result, sterile neutrinos, and low energy solar neutrino experiments, *Phys. Rev. D* 69 (2004) 113002.
- [33] P.C. de Holanda and A.Yu. Smirnov, Solar neutrino spectrum, sterile neutrinos, and additional radiation in the Universe, *Phys. Rev. D* 83 (2011) 113011.
- [34] Ilidio Lopes, The Sterile-Active Neutrino Flavor Model: The Imprint of Dark Matter on the Electron Neutrino Spectra, *Astrophys. J.* 869 (2018) 112.
- [35] V. Barger, Patrick Huber, and Danny Marfatia, Solar Mass-Varying Neutrino Oscillations, *Phys. Rev. Lett.* 95 (2005) 211802.
- [36] A. Friedland, et al., Solar neutrinos as probes of neutrino-matter interactions, *Phys. Lett. B* 594 (2004) 347–354.
- [37] O.G. Miranda, et al., Are solar neutrino oscillations robust?, *J. High Energy Phys.*, 10 (2006) 008.
- [38] Y. Takeuchi, et al., Development of high sensitivity radon detectors, *Nucl. Instrum. Meth. Phys. Res. Sect. A* 421 (1999) 334–341.
- [39] H. Sekiya, Quest for the lowest-energy neutrinos in Super-Kamiokande, *AIP Conf. Proc.* 1672 (2015) 080001.
- [40] I. Blevis, et al., Measurement of ^{222}Rn dissolved in water at the Sudbury Neutrino Observatory, *Nucl. Instrum. Meth. Phys. Res. Sect. A* 517 (2003) 139–153.
- [41] T.C. Andersen, et al., Measurement of radium concentration in water with Mn-coated beads at the Sudbury Neutrino Observatory, *Nucl. Instrum. Meth. Phys. Res. Sect. A* 501 (2003) 399–417.
- [42] B. Aharmim, et al., High sensitivity measurement of ^{224}Ra and ^{226}Ra in water with an improved hydrous titanium oxide technique at the Sudbury Neutrino Observatory, *Nucl. Instrum. Meth. Phys. Res. Sect. A* 604 (2009) 531–535.
- [43] M. Balata, et al., The water purification system for the low background counting test facility of the Borexino experiment at Gran Sasso, *Nucl. Instrum. Meth. Phys. Res. Sect. A* 370 (1996) 605–608.
- [44] H. Simgen, et al., A new system for the ^{222}Rn and ^{226}Ra assay of water and results in the Borexino project, *Nucl. Instrum. Meth. Phys. Res. Sect. A* 497 (2003) 407–413.
- [45] M.C. Chu, et al., The radon monitoring system in Daya Bay Reactor Neutrino Experiment, *Nucl. Instrum. Meth. Phys. Res. Sect. A* 808 (2016) 156–164.
- [46] Y.P. Zhang, et al., The development of ^{222}Rn detectors for JUNO prototype, *Radiat. Detect. Technol. Methods* 2 (2018) 5.
- [47] L. Xie, et al., Developing the radium measurement system for JUNO’s water Cherenkov detector, *arXiv:1906.06895*.
- [48] C. Mitsuda, et al., Development of super-high sensitivity radon detector for the Super-Kamiokande detector, *Nucl. Instrum. Meth. Phys. Res. Sect. A* 497 (2003) 414–428.
- [49] P. Kotrappa, S.K. Dua, P.C. Gupta, Y.S. Mayya, Electret - A New Tool for Measuring Concentrations of Radon and Thoron in Air, *Health Phys.* 46 (1981) 35.
- [50] Y. Nakano, et al., Measurement of radon concentration in Super-Kamiokande’s buffer gas, *Nucl. Instrum. Meth.*

- Phys. Res. Sect. A 867 (2017) 108–114.
- [51] K. Hosokawa, et al., Development of a high-sensitivity 80 L radon detector for purified gases, *Prog. Theor. Exp. Phys.* 033H01 (2015).
 - [52] J. Steyn, Absolute Standardization of Beta-emitting Isotopes with a Liquid Scintillation Counter, *Proc. Phys. Soci. Sec. A* 69 (1956) 865.
 - [53] M. Noguchi, Special Applications (2), Measurements of Radon Activity, *RADIOISOTOPES* 24 (1975) 745–748.
 - [54] Yumi Yasuoka, et al., Determination of Radon Concentration in Water Using Liquid Scintillation Counter, *RADIOISOTOPES* 53 (2004) 123–131.
 - [55] S. Maurer, A Mersmann and W. Peukert, Henry coefficients of adsorption predicted from solid Hamaker constants, *Chem. Eng. Sci.* 56 (2001) 3443–3453.
 - [56] Hardy Singen, Adsorption techniques for gas purification, *AIP Conf. Proc.* 785 (2005) 121.
 - [57] K. Abe, et al., Radon removal from gaseous xenon with activated charcoal, *Nucl. Instrum. Meth. Phys. Res. Sect. A* 661 (2012) 50–57.
 - [58] D.S. Akerlib, et al., Chromatographic separation of radioactive noble gases from xenon, *Astropart. Phys.* 97 (2018) 80–87.
 - [59] M. Ikeda, et al., Adsorption and desorption of radon in argon gas, and the development of low level radon concentration measurement method, *RADIOISOTOPES*, 59 (2010) 29–36.
 - [60] M. Shimo, et al., Experimental Study of Charcoal Adsorptive Technique for Measurement of Radon in Air, *J. Atom. Energy Soci. Jap.* Vol. 25 (1983) 562–570.
 - [61] T. Iida, et al., An Electrostatic Integrating ^{222}Rn Monitor with Cellulose Nitrate Film for Environmental Monitoring, *Health Phys.* 54 (1988) 139.
 - [62] E. Blaufuss, et al., ^{16}N as a calibration source for Super-Kamiokande, *Nucl. Instrum. Meth. Phys. Res. Sect. A* 458 (2001) 638–649.
 - [63] Y. Nakano, ^8B solar neutrino spectrum measurement using Super-Kamiokande IV, PhD thesis, University of Tokyo (2016), available at <http://www-sk.icrr.u-tokyo.ac.jp/sk/publications/index-e.html> (accessed on October 9th, 2019).
 - [64] Y. Nakano for the Super-Kamiokande Collaboration, Radon background study in Super-Kamiokande, *J. Phys. Conf. Ser.* 888 (2017) 012191.
 - [65] K. Abe, et al., Hyper-Kamiokande Design Report, arXiv:1805.04163.